IAC-08-C1.8.5

OPTICAL BEAM CONTROL FOR IMAGING SPACECRAFT WITH LARGE APERTURES

Jae Jun Kim
Research Assistant Professor, jki1@nps.edu
Anne Marie Johnson
NRC Research Associate, ajohnson@nps.edu
Brij N. Agrawal
Distinguished Professor, agrawal@nps.edu
Naval Postgraduate School, Monterey, CA 93943

ABSTRACT

This paper discusses optical beam control using adaptive optics for imaging spacecraft with large aperture telescopes. The segmented mirror alignment and active mirror surface control are achieved by novel wavefront sensing and control techniques. The experimental testbed and test results are also presented to demonstrate the adaptive optics techniques for large-aperture segmented mirrors.

1. INTRODUCTION

To meet demands for enhanced collection capability, many future imaging spacecraft will require mirror sizes of 5-10 m or greater in diameter. These mirrors, like the primary mirror on the James Webb Space Telescope (JWST), will be segmented and light weight and require on orbit deployment. Meeting mirror surface figure and alignment requirements to minimize optical beam wave front error is very challenging. The mirror surface could also have structure and control interactions. The coarse pointing of the optical beam is achieved by the spacecraft bus attitude control system. However, fine pointing and correction for aberrations in the optical beam due to mirror surface error, optical train imperfections and jitter is performed by the optical payload control system. One approach to correct mirror surface error is through the use of adaptive optics techniques. The JWST, for example, use adaptive optics for the alignment of mirror segments [1], [2]. The key technology challenges of the adaptive optics system for large aperture space-based segmented mirror such as JWST are development of robust wavefront sensing and mirror surface control techniques. Future imaging spacecraft may use adaptive optics for both alignment of the mirror segments and control of the segmented mirror surface figure. In this paper, a brief review of the recent work done at the Spacecraft Research and Design Center in this area is presented [3],

[4]. Segment alignment using a Redundant Spacing Calibration (RSC) wavefront sensing technique is presented. The challenge in the control design of the mirror surface figure control is identified. Experimental adaptive optics testbed are also presented including test results on RSC technique and mirror surface control.

2. ADAPTIVE OPTICS

The main purpose of an adaptive optics system is to improve the capability of an optical system by actively compensating for wavefront aberrations in real-time. An adaptive optics system consists of a wavefront sensor to measure the aberration of the incoming light, a compensation device such as an actuated deformable mirror, and a processor which interprets the sensor data in terms of the aberration profile and determines appropriate control actuation to the compensation device.

A wide range of wavefront sensors is available for adaptive optics. Among those, the Shack-Hartmann wavefront sensor consists of a lenslet array in front of an imaging sensor. Each lenslet focuses the incoming wavefront to a spot on the detector. The local wavefront slope at each lenslet determines the axial displacement of this spot. Therefore the centroids of each spot are found in x-y coordinates and by simple triangle geometry the wavefront gradient in x and y can be deduced. Modal or Zonal wavefront reconstruction can then be performed. The Phase Diversity curvature sensor is also commonly used for wavefront sensing. It measures the intensity profile of two imaging planes at different distances (chosen to provide an equal and opposite amount of defocus) along the propagation path to determine the curvature of a wavefront.

Wavefront compensation is achieved when the compensation-device applies a conjugate to the phase aberration. Micromachined Membrane Deformable Mirror (MMDM) and Piezoelectric Deformable Mirror (PDM) are commonly used to create the desirable mirror surface figure.

3. SEGMENT ALIGNMENT

3.1 Techniques

Currently, a range of wavefront sensors and other optical techniques are adopted for the alignment of mirror segments in space. For example, dispersed-fringe sensing, is used during initial telescope alignment for sensing large segment piston errors, while fine phasing control is periodically performed to correct segment phase from the order of several wavelengths to sub-wavelength accuracy [5]. This is achieved with more accurate and versatile sensors (capable of correcting tilt errors in addition to piston), for example curvature sensing, but this accuracy comes at the expense of dynamic range.

Using a different sensor modality for each alignment stage adds to the payload and significantly increases processing time, with multiple measurements and computationally intensive solution algorithms being necessary. A new wavefront sensing technique known as

Redundant Spacings Calibration (RSC) has recently been developed to simultaneously calibrate both relative pistons and tip-tilts with high dynamic range [6]. The basis for this technique had previously existed in a piston-only calibration format for the phase errors affecting synthesis imaging [7]. In addition to having the potential to deliver higher dynamic range, RSC can work with extended sources, wavefront solution is non-iterative and therefore significantly faster, and further advantage is offered in that measurements are made from the image itself (a single detector plane) thereby further reducing the onboard wavefront sensor equipment. The underlying principle is that by designing an aperture array to contain repeated (redundant) spacings, we can make simultaneous measurements of repeated spatial frequency content of the scene. In the absence of aberrations, these duplicate measurements should yield the same results. Therefore, any difference in measurements is solely due to aberrations. In this way, object phase can be separated from the aberration component without the need for a reference laser.

For a segmented mirror, light reflected from the mirror is passed through a redundantly designed aperture mask, each pair of apertures sampling a spatial frequency component of the object brightness distribution. Identical frequency components posses the same object phase, only differing in terms of the amount of aberration introduced by the instrument. The interferogram formed from this array is the frequency-limited image of the object and the contrast of this plane can be used to adaptively correct the segment phase by driving the mirror segments until maximum image sharpness is reached at a position of zero aberration. Alternatively, the recorded image can be Fourier transformed in real-time giving a complex plane of spatial frequency data from which the phase of individual frequency components can be extracted. It was shown in [6] how the phase part of the complex measurement data is related to the piston and tip/tilt coefficients of the mirror segments. Provided the aperture array is designed according to the criteria specified below, a number of such equations (one for each spacing) can be formed into a solvable system of simultaneous equations (usually in matrix form). The pseudo-inverse can then be applied to retrieve the coefficients, which can be used to adaptively correct the segment misalignment. The equations are

$$(c_k - c_j) + (a_k + a_j)\frac{x}{2} + (b_k + b_j)\frac{y}{2} = m_{jk}(x, y) \quad (1)$$

where c_j, a_j and b_j are the piston, and tilt coefficients respectively of aperture j, and $m_{jk}(x, y)$ is the measured phase in the image transform, for the j,k th aperture pair.

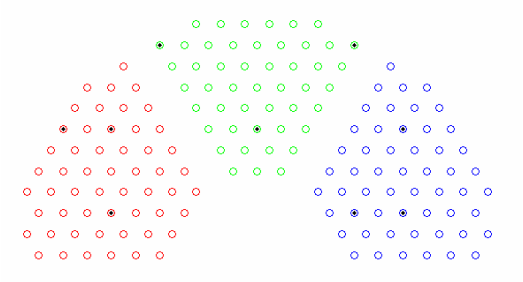

Fig. 1: Picture of an RSC aperture mask designed to calibrate 3 of the mirror segments

Aperture spacings were designed to allow unique identification of piston and tip-tilt for each segment in the array. The minimum number of apertures for this purpose is 3 per segment but the overall array of N apertures must contain N-3 repeated spacings for the system to be full-rank. Each spacing must be repeated only once otherwise phase extraction in the complex plane is compromised. A search algorithm based on a hexagonal, space filling geometry was developed to find acceptable positioning for apertures.

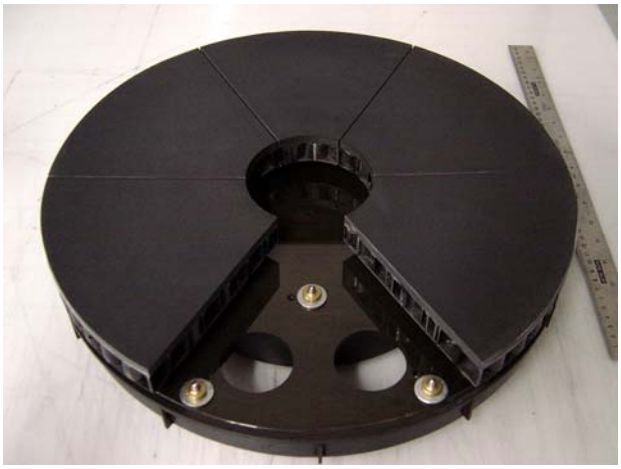

Fig. 2: 16 inch Segmented Mirror

Fig. 1 illustrates one such array compatible with the NPS 16 inch segmented mirror shown in Fig. 2. Only 3 segments were chosen to demonstrate the principle since a different experimental coating had been applied to the lower half of the mirror which would influence results.

3.2 Testbed

The NPS adaptive optics testbed shown in Fig. 3 is built to demonstrate adaptive optics methods for both mirror segment alignment and mirror surface control. The testbed employs a 16 inch parabolic carbon fiber segmented mirror and the each segment employs three lead screw actuators for tip/tilt and piston correction. The RSC wavefront sensor, consists of an aperture array mask and a CCD camera.

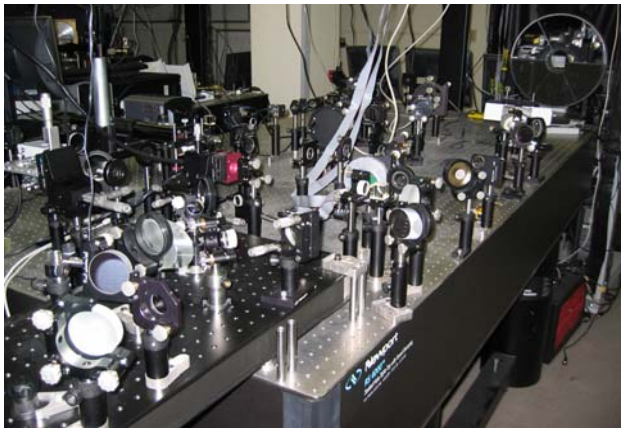

Fig. 3: Adaptive Optics Testbed

On laboratory propagation scales, the parabolic profile of the segmented mirror introduces spherical aberration into the phase of the reflected wavefront. We compensated for this static aberration by designing and constructing a null-corrector.

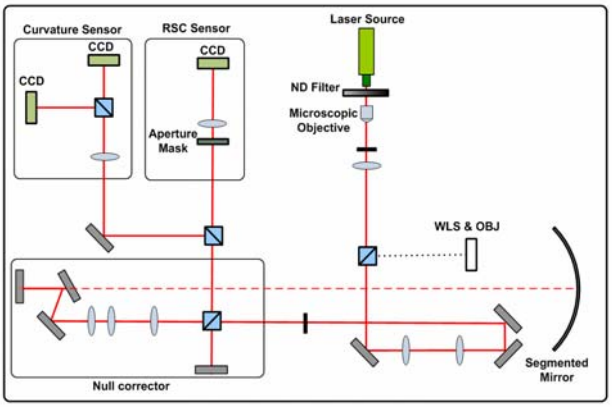

Fig. 4: Layout of the Testbed for Segmented Mirror Alignment Demonstration

For comparison with the RSC technique, a Curvature sensor has also been constructed on the testbed. Higher order surface aberration modes are currently being corrected using a Hartmann wavefront sensor but this method is insensitive to segment piston misalignment. The layout of the adaptive optics testbed is shown in Fig. 4.

3.3 Simulation and Experimental Results

Parabolic mirrors are designed to focus light originating at infinity to a single point but when a nearby extended source is used, the divergence of the light rays introduces spherical aberration upon reflection, preventing the light from being focused to a point. A singlet lens can be used in this case to provide an opposing aberration. A null corrector was designed and constructed by this principle. Fig. 5 shows the interferometric image of the segmented mirror pupil plane after the beam has passed through this null-corrector. In addition to the spherical aberration however it was found that relaxation effects of the mirror structure had caused additional aberration terms. This null corrector is therefore being replaced by one containing a liquid crystal spatial light modulator which could be programmed with more complex compensatory static aberrations. Preliminary, successful experimental results were obtained using the RSC sensor with a reference beam but at this time full experimental implementation of RSC using light from the extended source is pending until construction of the new null-corrector is complete.

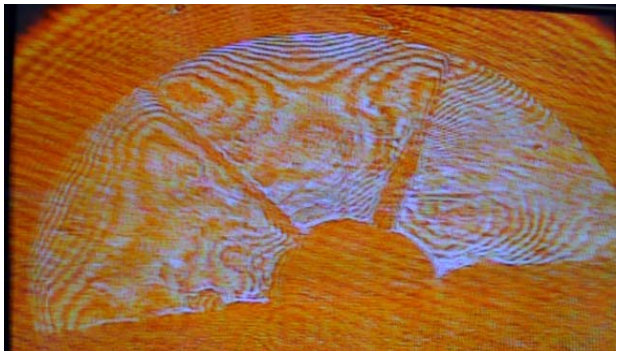

Fig. 5: Interferometric image of the segmented mirror pupil plane

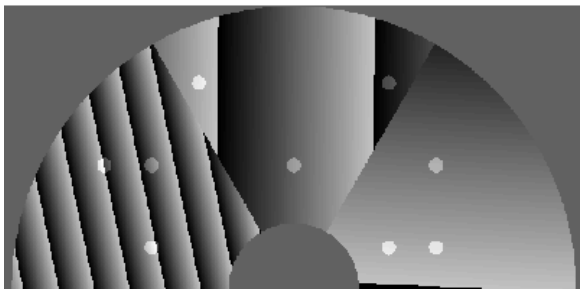

(a)

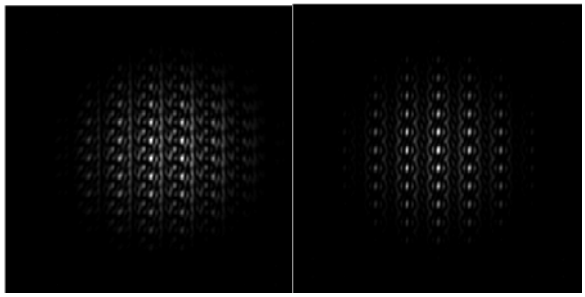

(b) (c)

Fig. 6: Aberrated phase profile of mirror segments with aperture locations superimposed (a), and corresponding interferogram (b), corrected interferogram (c)

A segmented pupil such as that shown in Fig. 6(a) was programmed to possess varying levels of piston and tip-tilt aberration. The aperture array of Fig. 1 (shown superimposed on to the

segments) was then used in generating the interferogram of Fig. 6(b). Taking the Fourier transform of this allows extraction of each aperture baseline phase component. Equation 1 from earlier describes the relationship between these components and the piston and tilt aperture coefficients. The matrix of these equations is solved by forming the pseudo-inverse and from these results the segment phases can be found. In simulation phase retrieval is achieved to the accuracy expected of the numerical transform operations.

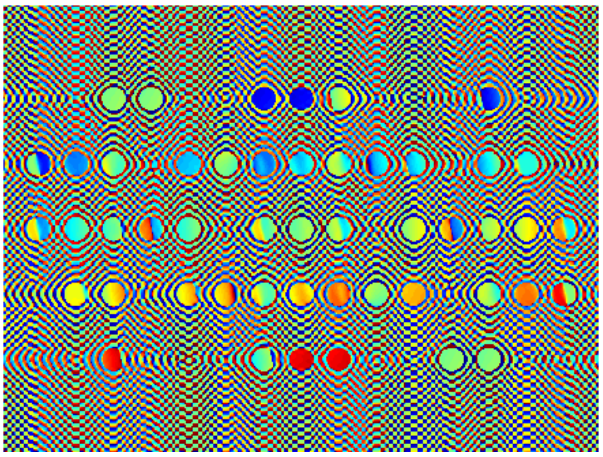

Fig. 7: The autocorrelation phase plane related to the image of Fig. 6(b) by Fourier transform.

4. SEGMENT SURFACE CONTROL

4.1 Techniques and Challenges

The adaptive optics system for mirror surface control can be represented by the following state-space equation.

$$\begin{aligned} \dot{x}(t) &= Ax(t) + Bu(t) \\ y(t) &= Cx(t) + Du(t) \end{aligned}, \qquad (2)$$

where, $x(t)$ is a state variable vector representing the mirror surface, $u(t)$ is a surface control input vector, and $y(t)$ is a sensor output vector. For adaptive optics systems with mirror face-sheet actuation, the typical number of control inputs and the sensor outputs are in hundreds or even in thousands. For example, the laboratory Shack-Hartmann wavefront sensor installed on the adaptive optics testbed measures 254 wavefront slopes in the x and y directions using a 127 lenslet array. The wavefront is then corrected by a 1-inch diameter Micromachined Membrane Deformable Mirror (MMDM) with 37 actuator inputs. In real systems, the number of inputs and outputs will likely be much larger than laboratory experiments. For large aperture space-based mirrors, the adaptive optics system is highly coupled between actuators, sensors and mirror segments due to its structural dynamics. When this dynamic coupling is ignored, problems could occur in achieving stable control. Therefore, this poses a challenging Multi-Input Multi-Output (MIMO) control problem with large number of inputs and outputs. In order to solve this control problem, model reduction of the original model will be needed. The MIMO, robust control design such as H-infinity control is currently under development.

When the dynamics of the deformable mirror is ignored, system equation in Equation 2 reduces to

$$y(t) = \Phi u(t) \quad \text{where, } \Phi = -CA^{-1}B + D \qquad (3)$$

Equation 3 represents the static relationship between the control input and the sensor output, and the matrix, Φ, is an influence coefficient matrix. With this simple static relationship, stabilization and regulation control of the wavefront can be achieved with integral control

or gradient based control method [8]. Since the dynamics of the mirror structure is ignored, structural filters are typically added in the aforementioned control design to minimize the structure and control interaction. However, the performance of the control design for large aperture space-based mirror will be limited without explicit consideration of mirror dynamics.

4.2 Testbed

In addition to the segmented mirror alignment demonstration, the adaptive optics testbed shown in Fig. 8 includes mirror surface control demonstration capabilities.

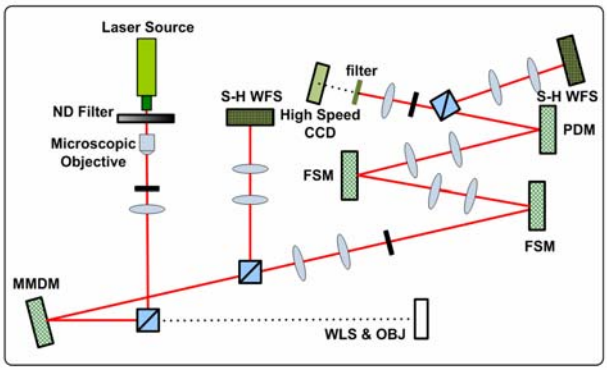

Fig. 8: Layout of the Testbed for Mirror Surface Control Demonstration

The testbed consists of three control systems: a primary deformable mirror control, a jitter control, and a secondary deformable mirror control. The 1-inch diameter MMDM with 37 actuators shown in Fig. 8 is used as a primary mirror. A Shack-Hartmann wavefront sensor with a 127 lenslet array is used as a wavefront sensing device for mirror surface control. The object light is passes through the same optical path as reference laser beam. The aberration measured in the perfect reference beam is created by the imperfection in the mirror surface. Therefore, imaging quality of the object light is improved by correcting the wavefront of the reference laser beam using a primary deformable mirror. The jitter control system is used to correct jitter in the optical beam generated by the spacecraft and simulated by the first fast steering mirror. This optical jitter is corrected by using a position sensing detector and fast steering mirror. The testbed has additional control loop with 1-inch Piezoelectric Deformable Mirror (PDM) with 27 actuators and a Shack-Hartmann wavefront sensor with a 127 lenslet array for the correction of any remaining aberration in the wavefront.

4.3 Experimental Results

Due to the size of the primary MMDM used in the experiment, dynamics of the mirror is beyond the sensor bandwidth. Therefore, only the static relationship shown in Equation 3 is considered in the control design. The experiment results are based on the primary mirror control system with the 1-inch MMDM and a Shack-Hartmann wavefront sensor. For the control design, integral control, gradient based control, and combined integral and gradient control methods are considered as follows.

$$\begin{aligned}
&\text{Integral Control:} && u(k+1) = u(k) - \mu\Phi^{\dagger} y(k) \\
&\text{Gradient Method:} && u(k+1) = u(k) - \mu\Phi^{T} y(k) \\
&\text{Combined:} && u(k+1) = u(k) - \mu_1\Phi^{\dagger} y(k) - \mu_2\Phi^{T} y(k)
\end{aligned} \tag{4}$$

There are two different approaches to apply

Equation 4: direct method and indirect method. The direct method explicitly estimates the phase of a wavefront. Therefore, the influence coefficient matrix used in Equation 4 should represent the static relationship between the control input and the phase output. With the indirect method, the influence coefficient matrix will represents the relationship between the control input and raw sensor output, which consists of wavefronts slopes from the Shack-Hartmann sensor in the experiment.

For the direct method for the control design, there are several ways to reconstruct the wavefront phase from the wavefront slopes. Zonal method is adapted for a specific sensor configuration, as the slope calculations depend on the grid pattern which is then used to determine the phase at each of the lenslet points. Another approach is to represent the phase of a wavefront using superimposition of Zernike modes, which can written as

$$\phi(r,\theta) = A_{00} + \frac{1}{\sqrt{2}}\sum_{n=2}^{\infty} A_{n0}\Re_n^0\left(\frac{r}{R}\right) + \sum_{n=1}^{\infty}\sum_{m=1}^{n}\left(A_{nm}\cos(m\theta) + B_{nm}\sin(m\theta)\right)\Re_n^m\left(\frac{r}{R}\right)$$

$$\Re_n^0\left(\frac{r}{R}\right) = \sum_{s=0}^{\frac{n-m}{2}}(-1)^s \frac{(n-s)!}{s!\left(\frac{n+m}{2}-s\right)!\left(\frac{n-m}{2}-s\right)!}\left(\frac{r}{R}\right)^{n-2s} \quad (5)$$

This modal representation of the wavefront phase can be obtained using phase points as a result of zonal method or, preferably, using the wavefront slope data and derivative of the Zernike modes.

Fig. 9 shows the reconstructed wavefront phase at the half-way biased MMDM position with spherical aberration.

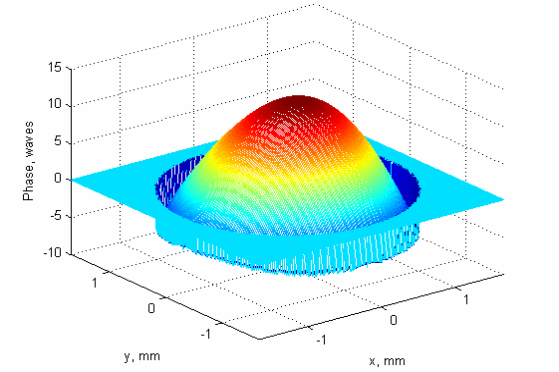

Fig. 9: Phase Using Initially Biased MMDM

Control Algorithm	Peak-to-Valley	RMS Error
Indirect Integral Control	0.266	0.143
Direct Integral Control (Zonal)	6.092	2.383
Direct Integral Control (Modal From Zonal)	0.268	0.086
Direct Integral Control (Modal from Zernike Derivatives)	0.082	0.028
Direct Gradient Method	0.736	0.199
Indirect Gradient Method	0.337	0.089
Direct Combined Integral control and Gradient Method	0.022	0.008

Table 1: Summary of Experimental Results for Different Control Design for Wavefront Correction

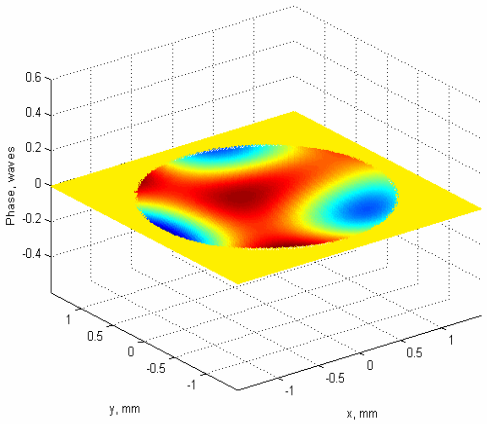

Fig. 10: Phase after Correction Using Combined Control (Peak-to-Valley = 0.0219)

It is shown in Table 1 that the combined integral control and gradient method provided the best performance for wave front correction with the smallest peak-to-valley value of the wavefront phase. Fig. 10 shows the corrected wavefront phase using the combined integral control and gradient method. The images of LED lighted object before wavefront correction (Fig. 9) and the after wavefront correction (Fig. 10) are also shown in Fig. 11 with improved imaging quality.

(a) Before (b) After

Fig. 11: Improvement in Imaging Quality

Next experiment is to study the effect of disturbance. The 2 Hz sinusoidal disturbance on the focus mode of the mirror is added to the mirror actuators. This additional input simulates vibrations due to flexible dynamics and disturbances from external sources. The discrete-time notch filter is added in the control design as

$$H_z(z) = \frac{1}{2}\left[1 + \frac{k_2 + k_1(1+k_2)z^{-1} + z^{-2}}{1 + k_1(1+k_2)z^{-1} + k_2 z^{-2}}\right] \quad (6)$$

where, $k_1 = -\cos(\omega_n)$ and $k_2 = \dfrac{1-\tan\left(\frac{BW}{2}\right)}{1+\tan\left(\frac{BW}{2}\right)}$.

Without additional structural notch filters, performance of the aforementioned control design degrades as illustrated in Fig. 12. With the addition of second order notch filter for every 37 actuators, the wavefront error is effectively reduced.

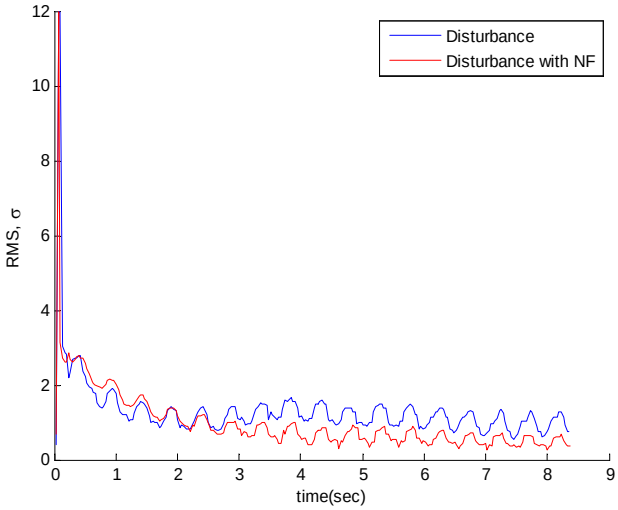

Fig. 12: RMS Error History for 2.0 Hz Sinusoidal Disturbance on Wavefront Focus Mode

5. CONCLUSION

In this paper, demonstration of segmented mirror alignment using RSC wavefront sensing method and mirror surface control is presented. The RSC method is capable of simultaneously retrieving relative piston and tip-tilt phase coefficients for the mirror segments and is expected to provide enhancement in dynamic range. It is also shown that the mirror surface control problem becomes a MIMO control with great number of control inputs and sensor outputs. The laboratory test results based on a static equation of a 1-inch MMDM shows improved imaging quality.

ACKNOWLEDGEMENT

The authors would like to thank for those who

have contributed their time and effort to the adaptive optics testbed. Contributors include Dr. Ty Martinez, Capt Matt Allen, and USAF, Maj Dan Burtz, USAF.

REFERENCES

[1] Dean, B. H., "Looking at Hubble through the Eyes of JWST", *2007 IEEE Aerospace Conference*, March 2007.

[2] Feinberg, L. D., et al, "TRL-6 for JWST wavefront sensing and control," Proceedings of SPIE, Vol. 6687, 2007.

[3] Allen, M., Kim, J. and Agrawal, B., "Control of a Deformable Mirror Subject to Structural Disturbance", SPIE Defense and Security Symposium, Orland, FL, March 2008.

[4] Agrawal, B. and Martinez, T., "Optical Beam Control Testbeds," AIAA Guidance, Navigation, and Control Conference and Exhibit, Honolulu, Hawaii, August 18-21, 2008.

[5] Redding, D., et al, "Performance of the NGST Wavefront Control System as Tested on DCATT",

[6] Johnson, A. M., Eastwood, R. J., Greenaway, A. H., "Calculation and Correction of Higher Order Phase Modes," JOSA A, in press

[7] Greenaway, A. H., "Terrestrial Optical Aperture Synthesis Technique (Toast)," Optics Communications, 58(3), 1986, pp.149-154.

[8] Zhu, L., Sun, P.C., Bartsch, D. U., Freeman, W. R., and Fainman, Y., "Adaptive control of a micromachined continuous-membrane deformable mirror for aberration compensation," Applied Optics, 38, 1999, pp.168-176.